Supplementary Information (SI) for Catalysis Science & Technology.
This journal is © The Royal Society of Chemistry 2025

Supporting Information

Enhancing the local electron density at active sites to promote the selective conversion of CO_2 into C_2H_6

Xinying Chen [a], Xinxin Jiang [a], Minlei Zhang [a], Tingyu Yang [a], Pengken Li[a], Jingran Yi [a], Yuming Dong [a*] and Yongfa Zhu[b]

[a]International Joint Research Center for Photo-responsive Molecules and Materials, School of Chemical and Material Engineering, Jiangnan University, Wuxi, 214122, China

[b]Department of Chemistry, Tsinghua Universty, Beijing, 100084, China

* E-mail: dongym@jiangnan.edu.cn (Yuming Dong)

Contents

1. Characterization

1.1 Photocatalytic CO_2RR activity

The photocatalytic CO_2RR was carried out in an airtight container by using a 300 W Xe lamp as a light source. In brief, 1000 mg/L catalyst suspension was prepared before testing. After sufficient ultrasonic dispersion, 5 mL catalyst suspension and 1.0 mL TEOA were mixed together and transferred to the reaction vessel. Before illumination, the high-purity CO_2 (99.999%) gas was injected into the closed system. Thereafter, the suspension was subjected to irradiation with full-spectrum light. The pressure was about 0.3 atm. The hydrocarbon fuel products were monitored by using a GC9790II (Fuli, China) and FID detector every two hours. The control experiments displayed that no obvious C_{2+} products could be detected under the reaction without a catalyst, the reaction in the dark, and the reaction with high-purity Ar gas instead of CO_2. In the stability test, we first had 5.0 mg of photocatalysts dispersed into 5 mL water. 5 mL above catalyst suspension and 1.0 mL TEOA were mixed and transferred to the reaction vessel. Before illumination, the high-purity CO_2 (99.999%) gas was injected into the closed system. Thereafter, the suspension was subjected to irradiation of light. After 4 h light irradiation, the first-used catalyst was washed with water and separated by a high-speed centrifuge. Parallel experiments were conducted to collect the first-used catalyst under the same condition, which could be used as a replenished catalyst in the second cycle. For catalyst regeneration, the first-used catalyst was dried at 60 °C in a vacuum overnight. In the second cycle, the replenished catalyst above was added. The parallel experiments for the second cycle were also carried out under the same conditions.

1.2 *In situ* EPR measurements

Room temperature electron paramagnetic resonance (EPR) spectra of the samples were measured with a paramagnetic resonance spectrometer ESR/EPR model Bruker EMXplus-6/1. Before testing, 5 mg/mL HCDS suspension (dispersed into methanol) needed to be prepared. Aqueous methanol solution dispersions were examined in sealed quartz tubes after argon bubbling for the “before photoactivation sample”. As the “after photoactivation sample”, the sealed quartz tube was irradiated by a Xe lamp for 30 min after argon bubbling. For the “after regeneration sample”, O_2 gas was purged to the “after photoactivation sample” for 30 min. All quartz tubes were frozen and stored in liquid nitrogen to maintain 77 K before EPR measurements.

1.3 *In situ* DRIFTS measurements

In situ Fourier transform infrared (*in situ* FT-IR) spectroscopy measurements were performed using on a Nicolet iS50 spectrometer (Thermo, USA) using the KBr pellet technique. Fourier-transform spectrometer equipped with a Harrick diffuse reflectance accessory at the Infrared Spectroscopy. Each spectrum was recorded by averaging 64 scans at 8 cm^{-1} spectral resolution. The chamber was sealed with two ZnSe windows. First, the silicon crystal is polished. Briefly, an appropriate amount of 0.5 μm alumina polishing powder is poured onto the polishing machine, and an appropriate amount of ultrapure water is added to make it evenly distributed, and rough polishing is performed at a rotational speed of about 300 or 500. Then, the above process was repeated and the polishing table was thoroughly cleaned before being polished with 0.05 μm silicon oxide polishing powder to achieve a smooth finish. The polished silicon crystals were put into a 50 mL beaker and sequentially sonicated with ultrapure water and ethanol for 5 min and rinsed with ultrapure water to obtain the polished silicon crystals. Next, sample solutions were prepared. 5.0 mg of catalyst was sonicated and dispersed in a mixture of 225 μL of ethanol and 25 μL of Nafion perfluorinated resin solution. The silicon crystals and the reaction cell were assembled and then 30 μL of the resulting suspension was uniformly added dropwise to the silicon crystals and dried under an infrared lamp. Finally, we added an appropriate amount of water solution to the reaction cell and connected it to the IR instrument. We tested the instrument by passing CO_2 through it and accessing the light source.

1.4 ***In situ*** **XPS measurement**

Synchrotron-radiation *in situ* XPS measurements were executed at the photoemission end-station at beamline BL11U in NSRL. The catalysts were treated in the preparation chamber, and subsequently transferred to the analysis chamber for XPS measurement without exposing it to air. In addition, the amount of surface Cu and N atoms within the same detection region was obtained from the calibrated Cu *2p* peak and N *1 s* peak areas. The tested areas were specimen charging by the incident photon flux and atomic ionization cross-sections at the corresponding X-ray energies.

2.Results and Discussion

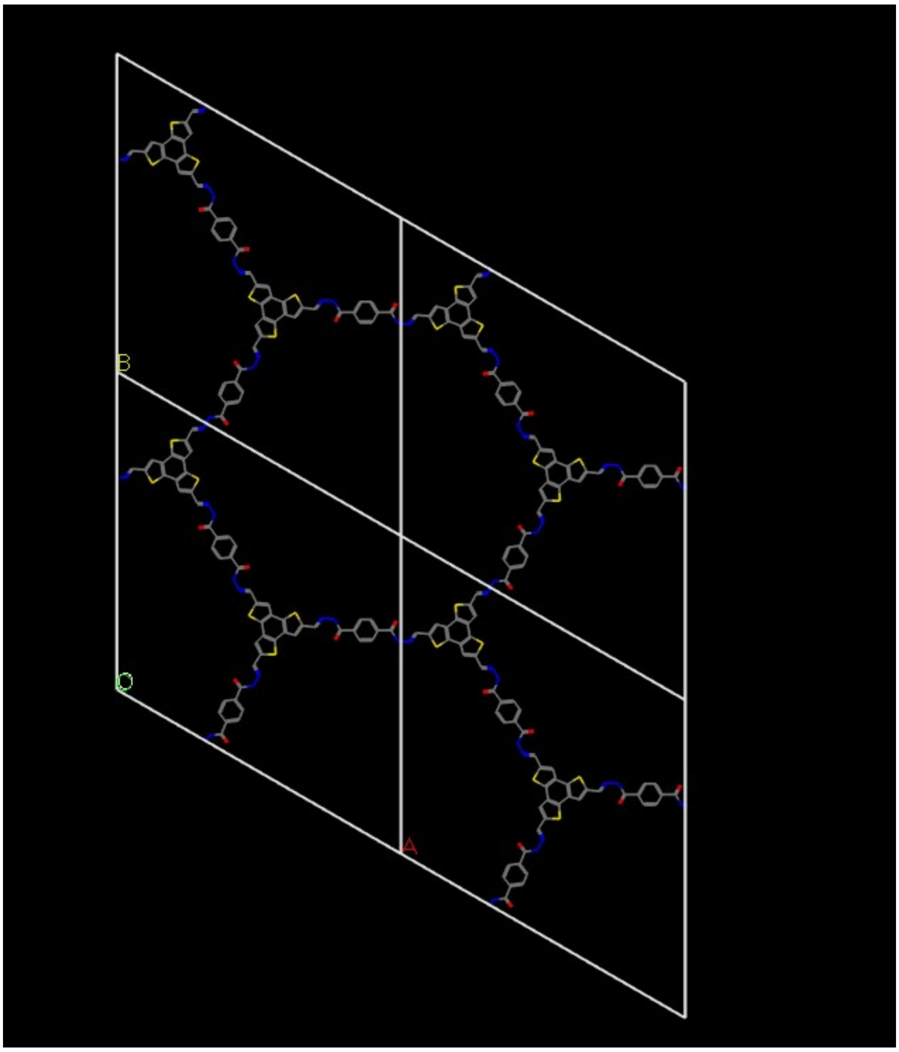

Fig. S1. The eclipsed DP-AA mode of BTT-DMTH-COF.

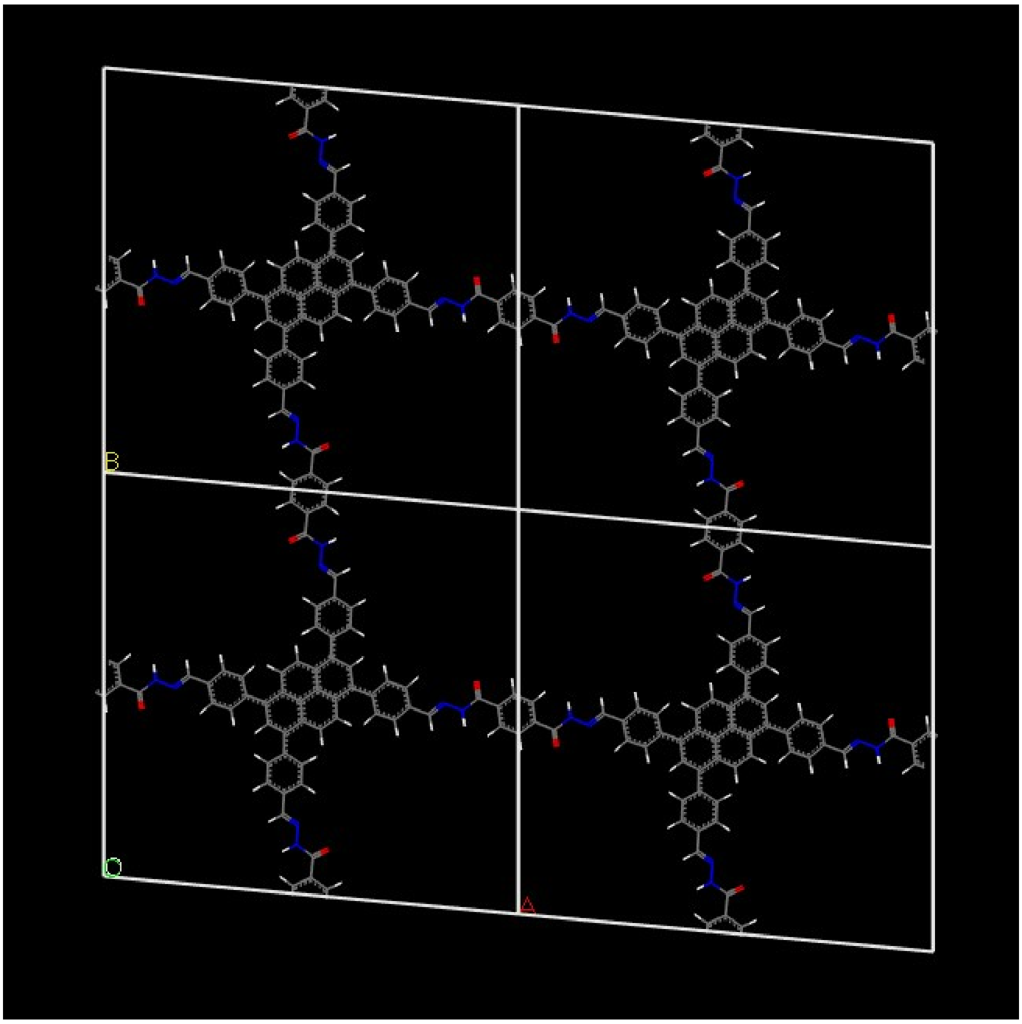

Fig. S2. The eclipsed DP-AA mode of Py-DMTH-COF.

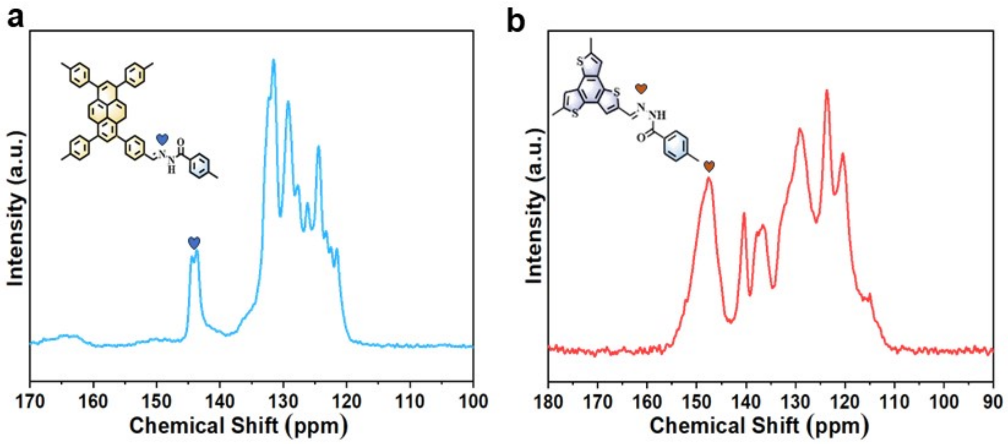

Fig. S3. Solid-state ^{13}C NMR spectra of (a) Cu@Py-DMTH-COF and (b) Cu@BTT-DMTH-COF.

Solid-state ^{13}C NMR spectra also confirmed the C=N bond was built on the Cu@Py-DMTH-COF and Cu@BTT-DMTH-COF, as revealed in Fig. S3a-b.

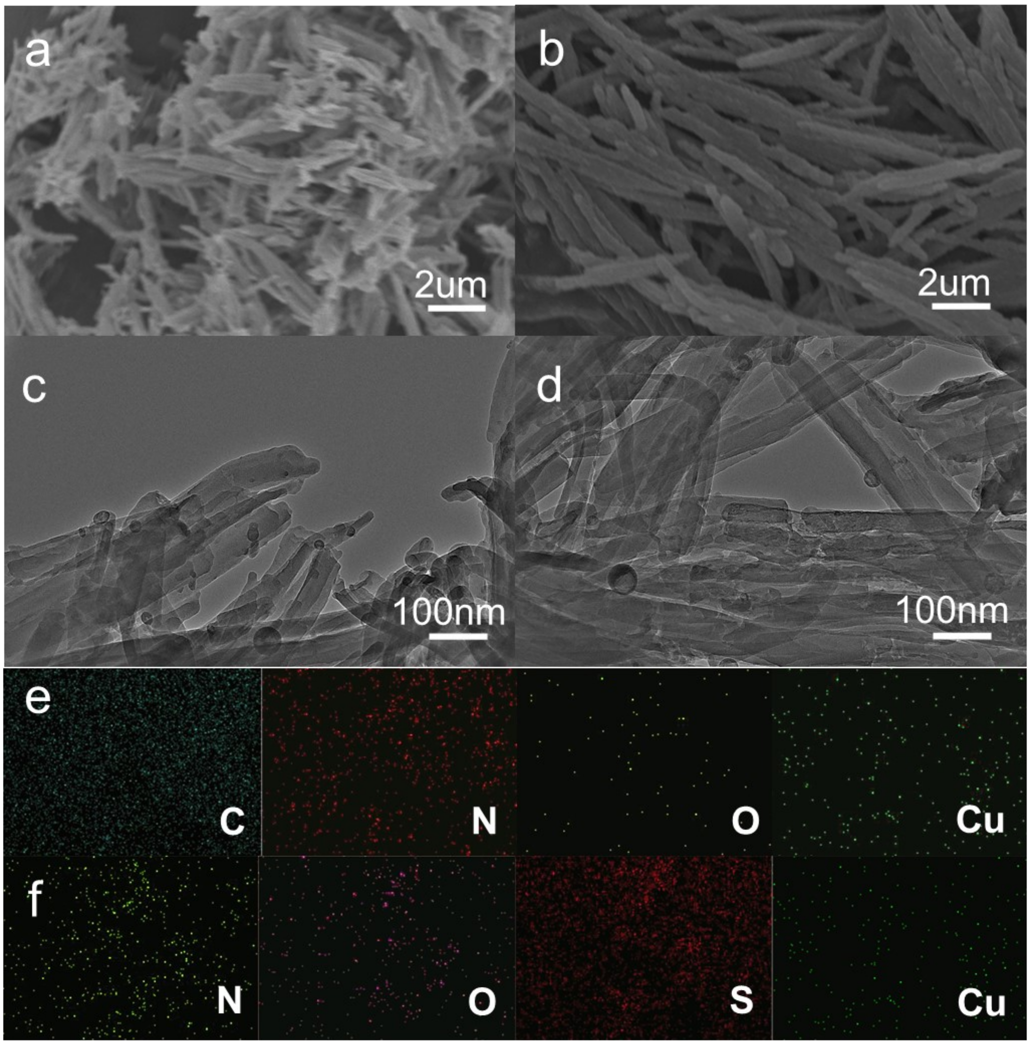

Fig. S4. (a) SEM image, (c) TEM image and (e) EDS mapping of Cu@Py-DMTH-COF; (b) SEM image, (d) TEM image (f) EDS mapping of Cu@BTT-DMTH-COF.

As shown in Fig. S4a-d, the SEM and TEM images of the Cu@Py-DMTH-COF and Cu@BTT-DMTH-COF depicted linear nanostrips from stacked elongated nanofibrils, arising from the lattice stripe spacing of the π-π stacking. In addition, energy-dispersive X-ray EDS affirmed the Cu sites was uniformly distributed on the Cu@Py-DMTH-COF and Cu@BTT-DMTH-COF (Fig. S4e-f).

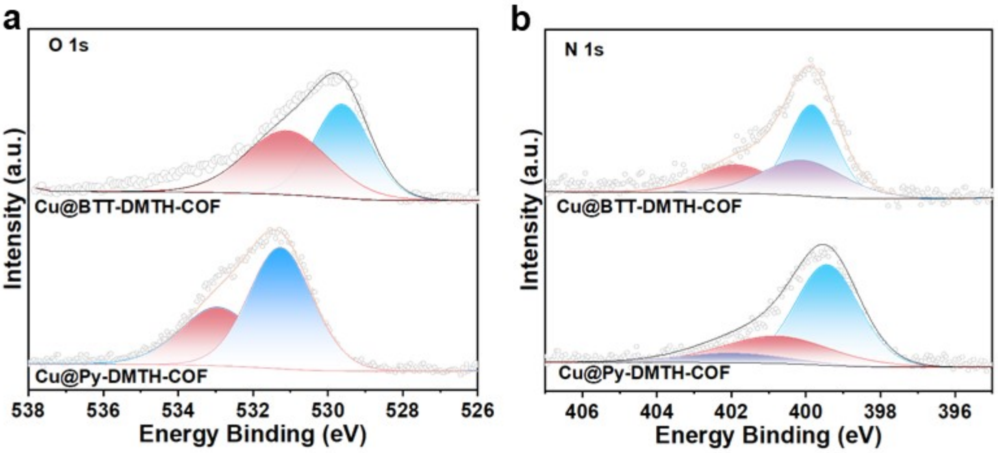

Fig. S5. (a) O *1 s* XPS spectra and (b) N *1 s* spectra of Cu@Py-DMTH-COF and Cu@BTT-DMTH-COF.

In the O *1 s* XPS spectra, the Cu@Py-DMTH-COF and the Cu@BTT-DMTH-COF showed two peaks of 531.7 and 530.1eV, respectively, which can be assigned to the C=O coordination (Fig. S5a). Importantly, the new peaks in O *1 s* XPS spectra and N *1 s* peaks were observed on the Cu@Py-DMTH-COF and Cu@BTT-DMTH-COF, which confirmed the Cu sites were coordinated with the O and N sites, thus promoting the charges transfer from COF into the Cu sites (Fig. S5b)

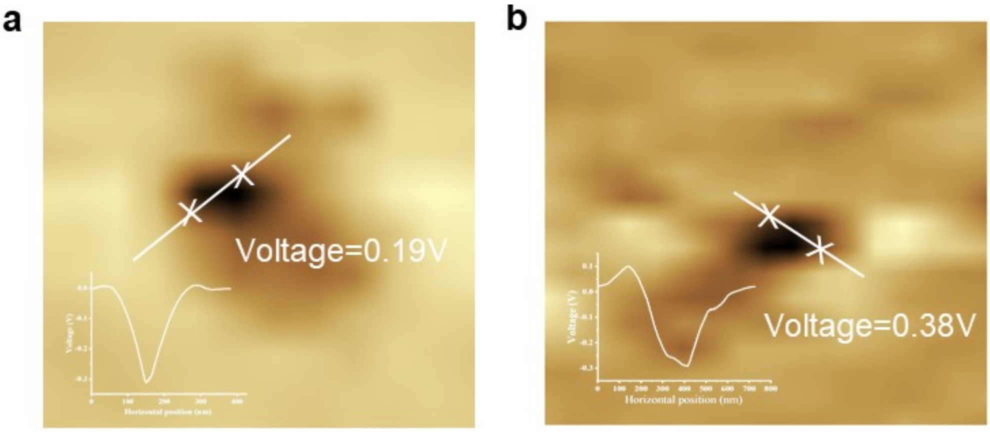

Fig. S6. KPFM images for (a) Cu@BTT-DMTH-COF and (b) Cu@Py-DMTH-COF.

As shown in Fig. S6, the KPFM results uncovered the lower surface potential on the Cu@BTT-DMTH-COF (0.19 V) than that of the Cu@Py-DMTH-COF (0.38 V).

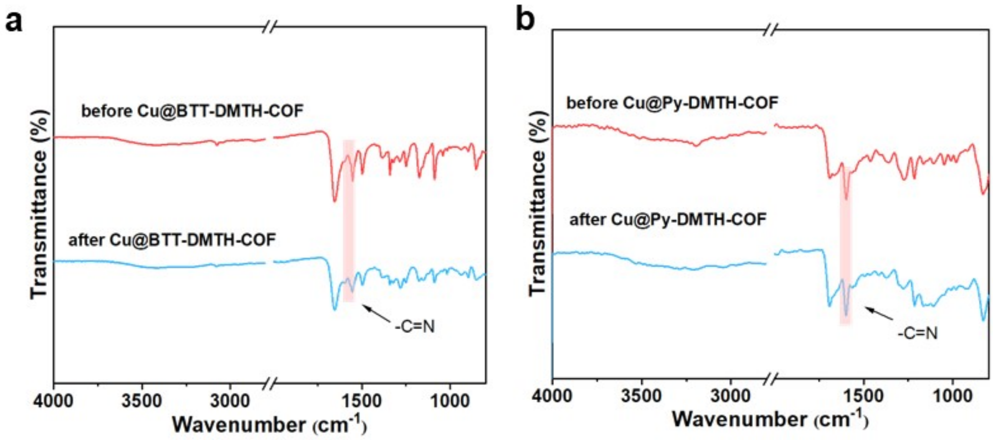

Fig. S7. FTIR spectra of the (a) Cu@BTT-DMTH-COF and (b) Cu@Py-DMTH-COF. before and after 4-cycling tests.

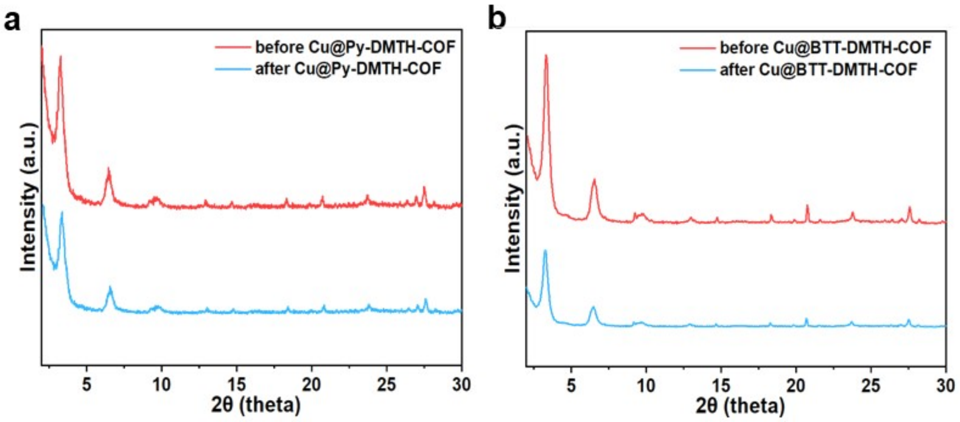

Fig. S8. XRD patterns of the (a) Cu@Py-DMTH-COF and (b) Cu@BTT-DMTH-COF before and after 4-cycling tests.

The XRD patterns and FTIR spectra remained unchanged after the 4-cycling tests, further illustrating the structural and morphological stability of the Cu@Py-DMTH-COF and Cu@BTT-DMTH-COF (Fig. S8 and S9).

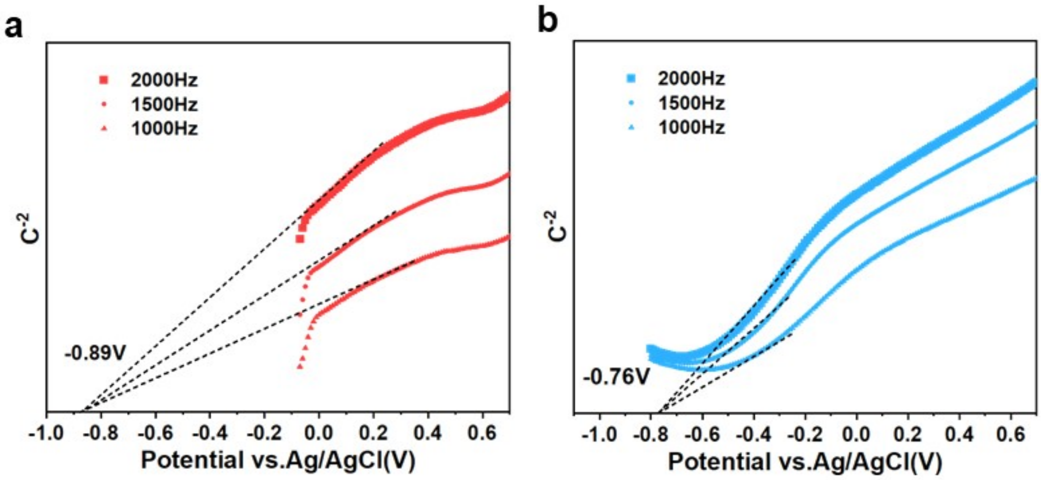

Fig. S9. Mott-Schottky plots for (a) the Cu@BTT-DMTH-COF and (b) Cu@Py-DMTH-COF.

The Mott-Schottky plots were carried out when using Ag/AgCl as the reference electrode. In that case, we can confirm that the conduction band was -0.89 eV and -0.76 eV vs. Ag/AgCl electrode for the Cu@BTT-DMTH-COF and Cu@Py-DMTH-COF.

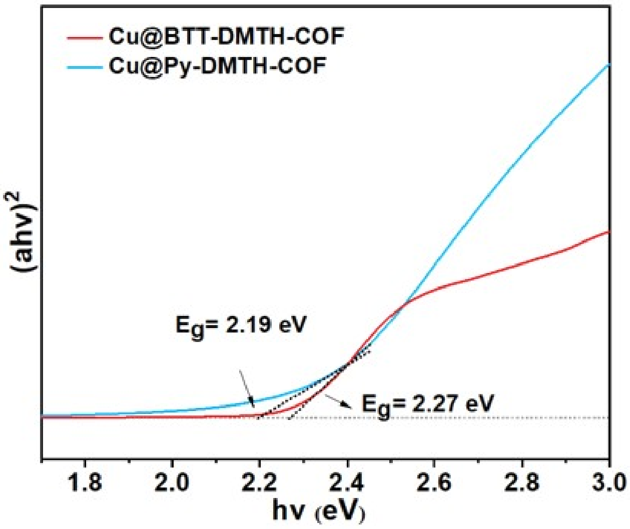

Fig. S10. Tauc structures of the Cu@Py-DMTH-COF and Cu@BTT-DMTH-COF.

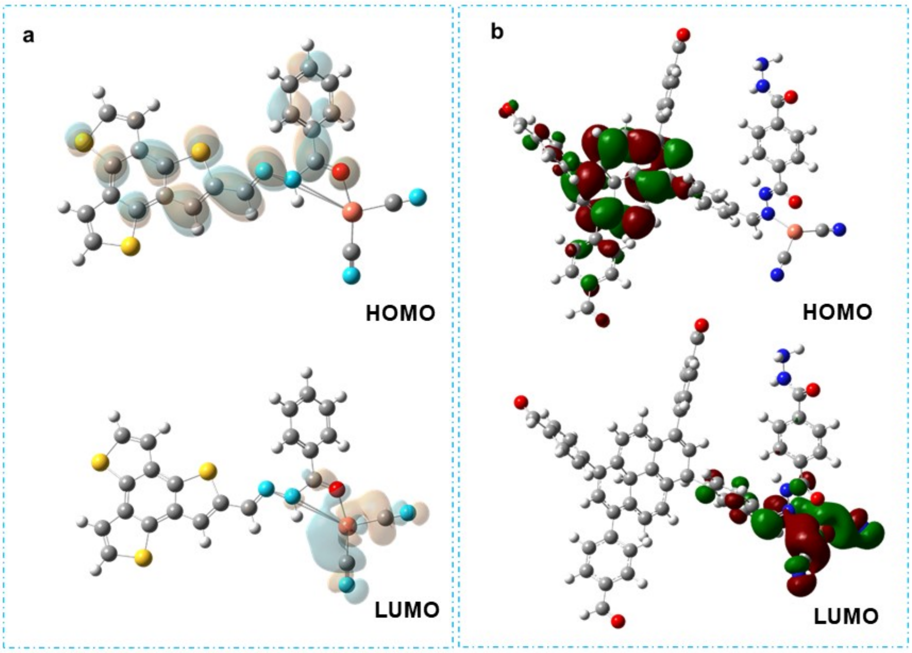

Fig. S11. Distributions of the highest occupied molecular orbital (HOMO) and the lowest unoccupied molecular orbital (LUMO), along with those of HOMO-1, HOMO and LUMO, LUMO+1 for the model system of (a) the Cu@BTT-DMTH-COF and (b) Cu@Py-DMTH-COF.

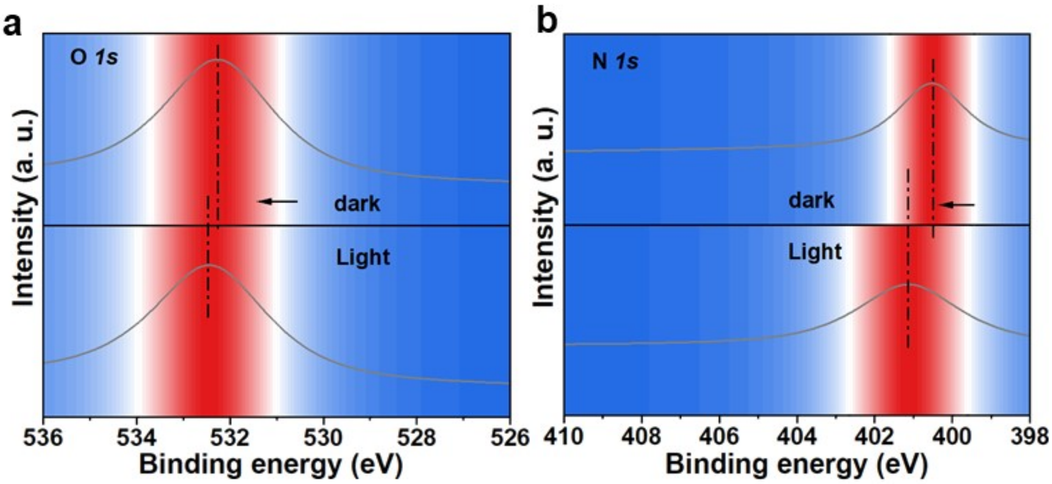

Fig. S12. (a) *In situ* O *1 s* XPS spectra and (b) *In situ* N *1 s* spectra of Cu@BTT-DMTH-COF.

The N *1 s* XPS peak and the O *1 s* XPS peak of Cu@BTT-DMTH-COF showed a upshift under irradiation, while the Cu *2p* XPS peaks downshifted, indicating the O and N sites was the electrons acceptors[1-3] (Fig. S13b-c).

Table S1. Fractional atomic coordinates for the unit cell of Py-DMTH-COF

Py-DMTH-COF space group: P1/m							
a=29.2 Å, b=28.3 Å, c=3.5 Å, α=β=90°, γ=95°							
Atom	x	y	z	Atom	x	y	z
C1	16.904	-7.268	0	N56	35.513	-14.602	0.001
C2	15.737	-8.04	0	C57	36.451	-13.713	0.001
C3	15.819	-9.433	0	O58	33.382	-16.357	0.001
C4	17.058	-10.099	0	N59	15.806	-23.415	0
C5	18.22	-9.297	0	N60	15.825	-24.814	0
C6	18.145	-7.903	0	C61	17.059	-25.535	0
C7	17.172	-11.522	0	O62	18.116	-24.926	0
C8	16.079	-12.436	0.001	N63	15.722	-5.173	0
C9	16.315	-13.837	0.001	N64	15.703	-3.774	0
C10	17.648	-14.332	0	C65	14.469	-3.053	0
C11	18.75	-13.429	0	C66	14.475	-1.58	0
C12	18.463	-12.06	0	O67	13.412	-3.662	0
C13	20.127	-13.807	0.001	C68	15.688	-0.879	0
C14	20.549	-15.149	0.001	C69	15.697	0.518	0
C15	21.904	-15.49	0.001	C70	14.492	1.234	0
C16	22.878	-14.492	0.001	C71	13.279	0.533	0
C17	22.487	-13.15	0	C72	13.27	-0.864	0
C18	21.132	-12.815	0	H73	14.717	-7.531	0
C19	14.756	-11.991	0.001	H74	14.866	-10.06	0
C20	13.69	-12.873	0.001	H75	19.25	-9.786	0
C21	13.88	-14.256	0.001	H76	19.101	-7.28	0
C22	15.212	-14.75	0.001	H77	19.311	-11.299	0
C23	15.449	-16.152	0.001	H78	19.779	-15.989	0.001
C24	16.772	-16.597	0	H79	22.215	-16.587	0.001
C25	17.838	-15.715	0	H80	23.276	-12.326	0
C26	12.777	-15.159	0.001	H81	20.815	-11.719	0
C27	13.065	-16.528	0.001	H82	14.53	-10.874	0.001
C28	14.356	-17.066	0.001	H83	12.621	-12.476	0.001
C29	11.4	-14.781	0.001	H84	16.997	-17.714	0
C30	14.469	-18.489	0.001	H85	18.906	-16.112	0
C31	10.978	-13.439	0.001	H86	12.216	-17.288	0.001
C32	9.624	-13.098	0.001	H87	11.749	-12.599	0.001
C33	8.65	-14.096	0.001	H88	9.313	-12.001	0.001
C34	9.041	-15.438	0.001	H89	8.252	-16.262	0.001
C35	10.396	-15.773	0.001	H90	10.713	-16.868	0.001
C36	15.709	-19.155	0	H91	16.678	-18.554	0
C37	15.791	-20.548	0	H92	16.809	-21.06	0
C38	14.624	-21.32	0	H93	12.426	-21.305	0.001

C39	13.382	-20.685	0.001	H94	12.291	-18.775	0.001
C40	13.307	-19.291	0.001	H95	13.713	-23.39	0
C41	14.679	-22.784	0	H96	24.584	-15.977	0.001
C42	24.292	-14.875	0.001	H97	17.815	-5.198	0
C43	16.849	-5.804	0	H98	26.829	-15.464	0.001
N44	25.23	-13.986	0.001	H99	28.501	-16.007	0.001
N45	26.571	-14.385	0.001	H100	30.913	-16.772	0.001
C46	27.626	-13.422	0.001	H101	32.242	-12.581	0.001
C47	29.031	-13.867	0.001	H102	29.83	-11.816	0.001
O48	27.361	-12.231	0.001	H103	33.934	-13.119	0.001
C49	29.339	-15.234	0.001	H104	36.185	-12.604	0.001
C50	30.67	-15.658	0.001	H105	14.871	-25.382	0
C51	31.712	-14.721	0.001	H106	16.656	-3.206	0
C52	31.404	-13.354	0.001	H107	16.672	-1.455	0
C53	30.073	-12.93	0.001	H108	16.688	1.082	0
C54	33.117	-15.166	0.001	H109	12.291	1.102	0
N55	34.172	-14.203	0.001	H110	12.279	-1.428	0

Table S2. Fractional atomic coordinates for the unit cell of Cu@BTT-DMTH-COF

Cu@BTT-DMTH-COF space group: P1/m							
a=37.3 Å, b=36.1 Å, c=3.5 Å, α=β=90°, γ=120°							
Atom	x	y	z	Atom	x	y	z
C1	16.904	-7.268	0	C40	34.089	-13.849	0.672
N2	15.737	-8.04	0	C41	40.452	-10.59	1.437
N3	15.819	-9.433	0	C42	39.232	-9.9	1.457
C4	17.058	-10.099	0	C43	38.023	-10.599	1.408
O5	18.22	-9.297	0	C44	38.018	-11.998	1.341
C6	18.145	-7.903	0	C45	39.238	-12.688	1.328
N7	17.795	-8.56	-0.152	C46	40.447	-11.989	1.373
O8	16.938	-10.704	-0.068	C47	28.79	-32.668	-0.61
N9	16.583	-7.843	-0.13	N48	29.866	-31.973	-0.767
C10	21.833	-11.77	-0.135	N49	29.753	-30.591	-0.948
C11	21.687	-10.375	-0.121	C50	30.898	-29.749	-1.075
C12	20.415	-9.796	-0.109	O51	32.016	-30.238	-1.089
C13	19.269	-10.603	-0.111	C52	30.168	-24.04	-1.255
C14	19.415	-11.997	-0.123	N53	31.313	-23.181	-1.143
C15	20.687	-12.576	-0.136	O54	29.045	-23.572	-1.338
C16	28.139	-14.229	0.056	N55	31.281	-21.786	-0.961
C17	26.892	-14.8	-0.128	C56	30.19	-21.095	-0.872
S18	26.885	-16.503	-0.39	C57	30.72	-28.29	-1.164
C19	32.652	-15.792	0.188	C58	31.828	-27.432	-1.174
C20	32.774	-14.439	0.432	C59	31.647	-26.047	-1.216

S21	31.299	-13.548	0.446	C60	30.356	-25.501	-1.252
C22	30.246	-19.65	-0.653	C61	29.249	-26.36	-1.252
S23	31.731	-18.813	-0.413	C62	29.431	-27.743	-1.206
C24	29.103	-18.869	-0.606	C63	15.424	-8.403	0.016
C25	29.106	-15.198	-0.019	C64	8.422	-6.719	0.408
C26	28.584	-16.462	-0.259	C65	8.325	-8.077	0.631
C27	31.335	-16.112	0.012	S66	9.815	-8.943	0.621
C28	30.492	-15.019	0.125	C67	11.908	-3.57	-0.381
C29	30.817	-17.387	-0.244	C68	10.746	-2.812	-0.403
C30	29.449	-17.561	-0.373	S69	9.285	-3.676	-0.156
C31	44.358	-8.693	0.861	C70	14.193	-7.61	0.02
N32	44.225	-9.959	1.097	S71	14.171	-5.903	-0.219
N33	42.97	-10.559	1.319	C72	12.958	-8.203	0.211
C34	41.725	-9.85	1.454	C73	9.733	-6.373	0.229
O35	41.714	-8.638	1.584	C74	10.595	-7.453	0.318
C36	36.745	-12.734	1.263	C75	11.589	-4.887	-0.157
N37	35.503	-12.013	1.172	C76	10.226	-5.087	-0.014
O38	36.755	-13.954	1.275	C77	12.474	-5.973	-0.068
N39	34.241	-12.592	0.935	C78	11.975	-7.249	0.162

References

1. Zheng, K.; Wu, M.; Zhu, J.; Zhang, W.; Liu, S.; Zhang, X.; Wu, Y.; Li, L.; Li, B.; Liu, W., Breaking the Activity–Selectivity Trade-off for CH_4-to-C_2H_6 Photoconversion. *Journal of the American Chemical Society* **2024,** *146* (17), 12233-12242.
2. Zheng, K.; Liu, S.; Li, B.; Zhu, J.; Zhang, X.; Wu, M.; Li, L.; Zhu, S.; Liu, W.; Hu, J., Atomically Precise Pd Species Accelerating CO_2 Hydrodeoxygenation into CH_4 with 100% Selectivity. *Precision Chemistry* **2023,** *1* (9), 530-537.
3. Wu, Y.; Wu, M.; Zhu, J.; Zhang, X.; Li, J.; Zheng, K.; Hu, J.; Liu, C.; Pan, Y.; Zhu, J., Spatially-separated redox sites enabling selective atmospheric CO_2 photoreduction to CH_4. *Science China Chemistry* **2023,** *66* (7), 1997-2003.